Feeding Compact Objects: Accretion on All Scales
Proceedings IAU Symposium No. 290, 2012
C. M. Zhang, T. Belloni, M. Méndez & S. N. Zhang, eds.

doi:10.1017/S1743921312019114

Multi-Wavelength Studies of the GX 339−4 2010 outburst

Marion Cadolle Bel[1], S. Corbel[2], A. Veledina[3], J. Rodriguez[2], P. D'Avanzo[4], J. Tomsick[5], D. M. Russell[6] and F. Lewis[7]

[1]ESAC/ISOC, Spain; email: Marion.Cadolles@sciops.esa.int; [2]AIM & CEA-Saclay, France; [3]Oulu Univ., Finland; [4]INAF, Italy; [5]SSL/California Univ., USA; [6]Tenerife Obs., Spain; [7]FT project, Glamorgan Univ., Wales

Abstract. The microquasar GX 339−4 experienced an outburst in 2010. We focus on observations that are quasi-simultaneous with those made by *INTEGRAL* and *RXTE* in March–April 2010 with radio, NIR, optical and UV data. X-ray transients are extreme systems, often harboring a black hole, known to emit throughout the whole electromagnetic spectrum in outburst. We studied the source evolution and correlated changes in all wavelengths. The bolometric flux increased from 0.8 to 2.9 $\times 10^{-8}$ erg cm^{-2} s^{-1} while the relative contribution of the hot medium decreased. The radio, NIR and optical emission from jets was detected and observed to fade as the source softened; reprocessing in the disc was strong at the end.

Keywords. Black hole physics, stars: GX 339−4 gamma rays, IR, radio: general, X-rays: binaries

1. Introduction

X-ray transients (XTs) are accreting low-mass X-ray binaries (LMXBs) that spend most of their time in a faint, quiescent state. They undergo large amplitude outbursts with rise times of only a few days or weeks (or months in the case of GX 339−4), with typical recurrence periods of many years (Tanaka & Shibazaki 1996). Based on the relative strengths of each spectral component, the degree of variability, shape of the PDS and on the properties of the radio emission in outburst, different spectral states have been defined (e.g., the low/hard (LHS) and the high/soft (HSS) main canonical states, McClintock & Remillard 2006; Homan & Belloni 2005). GX 339−4 is a recurrent XT with regular outbursts. We triggered *INTEGRAL* during the initial hard X-ray phase (Tomsick 2010; Prat *et al.* 2010), and in the declining phase (Cadolle Bel *et al.* 2010). We report and discuss some of the results of this multiwavelength campaign.

2. Observations and Data Analysis

Figure 1 (left) shows the *RXTE*/ASM, *SWIFT*/BAT X-ray and *INTEGRAL* light curves of the outburst (other multi-wavelength observations indicated). The IBIS/ISGRI and JEM-X data were reduced using standard analysis procedures of the off-line scientific analysis `OSA 9.0` following standard procedures (e.g., Rodriguez *et al.* 2008; Cadolle Bel *et al.* 2009). The *RXTE* data were reduced with the `HEASOFT` software package v6.10, following standard procedures (see Rodriguez *et al.* 2008). All Swift/XRT observations discussed in this paper were made in window timing (WT) mode to avoid pile-up due to the source brightness. In addition, data were collected from the *Swift*/UVOT (UV and optical) instrument, with MJD spanning from 55217 to 55310. Optical and NIR observations were performed with the REM telescope (see, e.g., Zerbi & The Rem Team 2001; Chincarini *et al.* 2003; Covino *et al.* 2004); optical data were also collected using the

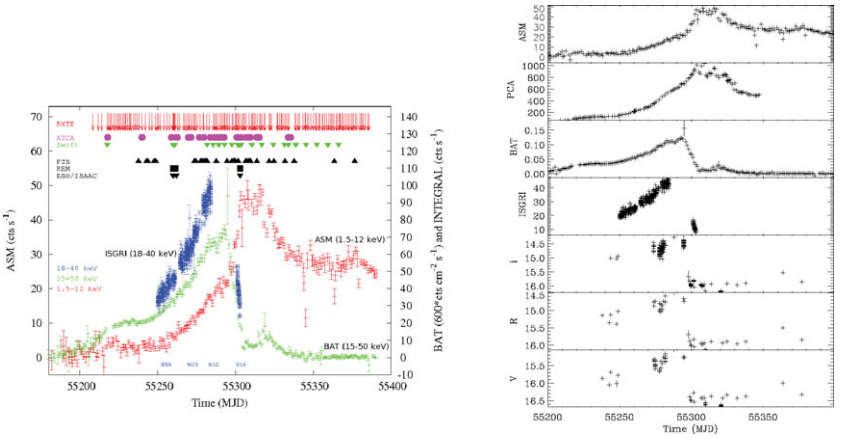

Figure 1. *Left:* Daily *RXTE*/ASM, *Swift*/BAT and *INTEGRAL*/ISGRI light curves of GX 339−4 during the 2010 outburst. Other observations performed with ATCA, the FTS, the REM/ROSS, REMIR and the ESO/ISAAC telescopes are indicated.The numbers near the bottom of the figure are *INTEGRAL* revolutions. *Right: RXTE*/ASM (cts s^{-1} in 1.5–12 keV), PCA (cts s^{-1} in 3–30 keV), *Swift*/BAT (cts cm^{-2} s^{-1} in 15–50 keV), *INTEGRAL*/ISGRI (cts s^{-1} in 40–80 keV) and FTS light curves (filters V, R and i').

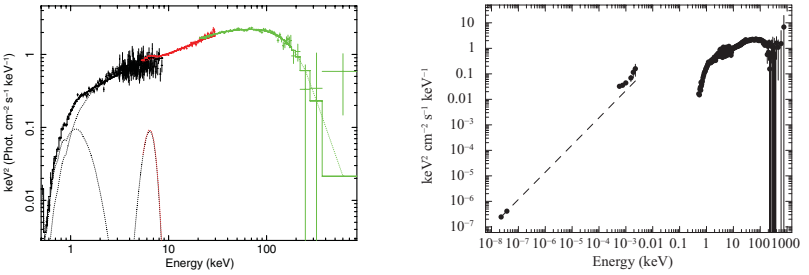

Figure 2. *Left: Swift*/XRT, *RXTE*/PCA and *INTEGRAL*/ISGRI LHS spectra of GX 339-4 (MJD ∼ 55259.9–55261.1; see text for fits). *Right:* SED from radio to soft γ-ray data, MJD ∼ 55259.9–55261.1 (Rev. 902). The dashed line is a simple power-law extrapolation of the two radio data points up to the NIR frequencies (this is not a physical model, but only shown for visual purpose).

2-metre robotic Asutralian Faulkes Telescope South (FTS). All science images were produced using an automatic pipeline that de-biases and flat-fields the raw images. Finally, GX 339−4 was frequently observed at radio frequencies with the ATCA; fluxes were 9.02±0.10 mJy, 9.56±0.05 mJy on MJD 55261.89 then 8.16±0.05 mJy and 7.94±0.10 mJy on MJD 55262.91 at, respectively, 5.5 and 9.0 GHz.

3. Results

Fig. 1 (right) presents the light curves obtained with the ASM (2–10 keV), PCA (3–30 keV), BAT (15–40 keV), ISGRI (40–80 keV) and FTS (V, R and i' magnitudes) instruments. The source shows the typical behaviour of an XT: the outburst started in hard X-rays probably around MJD ∼ 55199. Around MJD 55295, the hard X-rays reached their peak and the emission began to decrease (with a secondary peak at MJD 55319) while the source continued to increase in soft X-rays until MJD 55327, before decreasing. This behaviour indicates a state transition from a hard to a softer state. The optical also dropped at the start of the transition, as reported in previous outbursts (Homan *et al.* 2005; Coriat *et al.* 2009). While during MJD 55259.9–55261.1 (Rev. 902) the source was still in a hard state, during MJD 55301.1–55303.3 (Rev. 916) GX 339−4

https://doi.org/10.1017/S1743921312019114 Published online by Cambridge University Press

Table 1. Best-fit spectral parameters around the period of our main *INTEGRAL* observations.

Time (MJD-55000)	Observations (Rev. #)	Disc Norm.	$kT_{\rm in}$ (keV)	$kT_{\rm e}$ (keV) or Γ	τ	$E_{\rm Fe\ line}$ (keV)	$\omega/2\pi$	$\chi^2_{\rm red}$ (dof)	F^a	$F^b_{\rm bol}$
217.7–217.8	N.A.	33784^{+28803}_{17644}	0.18 ± 0.01	$\Gamma=1.62\pm0.02$	-	$6.53^{+0.32}_{-0.35}$	$0.34^{+0.10}_{-0.08}$	1.45 (281)	1.43	N.A.
237.5–240.2	895[c]	35^{+20}_{-9}	0.83 ± 0.10	41^{+5}_{-4}	$1.63^{+0.14}_{-0.17}$	$6.56^{+0.20}_{-0.25}$	0.25 ± 0.05	0.84 (97)	1.99	0.82
240.7–243.2	896[c]	100^{+186}_{-50}	$0.67^{+0.02}_{-0.11}$	38^{+4}_{-3}	$1.69^{+0.13}_{-0.14}$	$6.15^{+0.21}_{-0.15}$	$0.19^{+0.05}_{-0.04}$	1.05 (102)	2.19	0.89
243.7–246.2	897[c]	100 ± 50	0.65 ± 0.10	41^{+5}_{-3}	$1.53^{+0.12}_{-0.15}$	$6.00^{+0.14}$	0.21 ± 0.03	1.13 (103)	2.14	0.86
246.7–249.1	898[c]	100^{+91}_{-50}	$0.64^{+0.03}_{-0.07}$	39^{+6}_{-3}	$1.59^{+0.14}_{-0.15}$	$6.00^{+0.25}$	0.22 ± 0.05	1.14 (102)	2.29	0.92
249.7–252.1	899[c]	66^{+252}_{-29}	$0.75^{+0.14}_{-0.20}$	40^{+5}_{-3}	$1.59^{+0.13}_{-0.15}$	6.37 ± 0.20	0.26 ± 0.05	1.09 (102)	2.49	1.02
252.5–255.1	900[c]	102 ± 51	$0.68^{+0.13}_{-0.19}$	39^{+4}_{-3}	$1.59^{+0.13}_{-0.15}$	$6.17^{+0.23}_{-0.49}$	$0.25^{+0.05}_{-0.04}$	0.78 (102)	2.74	1.09
255.6–258.1	901[c]	124^{+388}_{-56}	$0.70^{+0.11}_{-0.16}$	45^{+7}_{-4}	$1.36^{+0.14}_{-0.17}$	$6.31^{+0.30}_{-0.70}$	0.32 ± 0.04	0.99 (102)	3.18	1.25
259.9–261.1	902	82887^{+63704}_{-38606}	0.19 ± 0.01	38^{+3}_{-2}	$1.49^{+0.10}_{-0.11}$	$6.23^{+0.15}_{-0.23}$	0.25 ± 0.04	1.58 (333)	3.38	1.64
264.5–267.1	904[c]	134^{+441}_{-57}	$0.73^{+0.12}_{-0.18}$	39^{+4}_{-3}	$1.45^{+0.11}_{-0.13}$	$6.23^{+0.29}_{-0.66}$	$0.34^{+0.05}_{-0.04}$	1.07 (102)	4.21	1.51
267.6–270.1	905[c]	183^{+1406}_{-87}	$0.67^{+0.12}_{-0.20}$	41^{+5}_{-3}	$1.31^{+0.12}_{-0.14}$	$6.27^{+0.27}_{-0.70}$	0.35 ± 0.04	1.11 (102)	4.60	1.61
270.4–272.8	906[c]	370^{+1664}_{-199}	$0.60^{+0.11}_{-0.13}$	38^{+4}_{-3}	$1.40^{+0.11}_{-0.12}$	$6.07^{+0.30}_{-0.47}$	$0.32^{+0.04}_{-0.03}$	1.33 (102)	5.04	1.77
273.4–276.0	907[c]	198^{+568}_{-71}	$0.68^{+0.09}_{-0.15}$	39^{+4}_{-3}	$1.28^{+0.11}_{-0.13}$	$6.45^{+0.19}_{-0.50}$	$0.35^{+0.05}_{-0.04}$	1.59 (102)	5.67	1.98
276.4–278.8	908[c]	338^{+2463}_{-174}	$0.62^{+0.13}_{-0.17}$	37^{+4}_{-3}	$1.28^{+0.11}_{-0.13}$	$6.29^{+0.35}_{-0.65}$	0.39 ± 0.06	1.15 (102)	6.59	2.15
279.4–281.5	909	32816^{+33761}_{-19118}	$0.21^{+0.02}_{-0.01}$	39^{+4}_{-3}	$1.16^{+0.11}_{-0.13}$	$6.23^{+0.15}_{-0.25}$	0.39 ± 0.04	0.88 (312)	7.80	2.79
281.7–281.8	N.A.	52^{+24}_{-20}	0.85 ± 0.09	$\Gamma=1.80\pm0.01$	-	$6.27^{+0.16}_{-0.22}$	0.38 ± 0.06	0.57 (255)	7.94	N.A.
282.4–284.9	910[c]	32^{+23}_{-6}	$1.19^{+0.10}_{-0.11}$	40^{+4}_{-3}	1.14 ± 0.12	$6.00^{+0.58}$	0.49 ± 0.04	0.96 (96)	7.69	2.25
289.3–289.6	N.A.	$840436^{+118692}_{-505374}$	$0.16^{+0.02}_{-0.01}$	$\Gamma=1.79\pm0.03$	-	$6.14^{+0.21}_{-0.29}$	0.28 ± 0.07	1.34 (228)	9.65	N.A.
297.8–297.9	N.A.	174096^{+86620}_{-62284}	0.22 ± 0.01	$\Gamma=1.95\pm0.02$	-	$6.00^{+0.04}$	0.10 ± 0.05	1.32 (260)	11.4	N.A.
301.1–303.3	916	3196^{+367}_{-288}	0.61 ± 0.02	256^{+6}_{-83}	$0.01^{+0.02}_{-0.01}$	$6.00^{+0.22}$	$0.51^{+0.09}_{-0.10}$	1.91 (252)	12.2	2.93
303.6–303.8	N.A.	2652^{+526}_{-353}	0.73 ± 0.04	35^{+5}_{-14}	$0.50^{+0.28}_{-0.50}$	$6.74^{+0.16}_{-0.14}$	$0.36^{+0.44}_{-0.32}$	1.77 (192)	14.6	N.A.
310.6–310.7	N.A.	999^{+45}_{-44}	$1.00^{+0.02}_{-0.01}$	$\Gamma=2.33^{+0.06}_{-0.07}$	-	$6.15^{+0.08}_{-0.09}$	-	1.50 (178)	13.3	N.A.

Notes: Models applied in `XSPEC` notations: CONSTANT*PHABS*REFLECT*(DISKBB+GAUSSIAN+POWERLAW) or CONSTANT*PHABS*REFLECT*(DISKBB+GAUSSIAN+COMPTT) (not all components always needed). Γ is the photon index. $N_{\rm H}$ varied between 4.9–6.3 $\times$ 10^{21} cm^{-2}. Errors are given at the 90% confidence level ($\Delta\chi^2 = 2.7$). a) Computed in the 2–20 keV range. Units: 10^{-9} erg cm^{-2} s^{-1}. b) X-ray bands extrapolated in the 0.01 keV–10 MeV range. Units: 10^{-8} erg cm^{-2} s^{-1}. c) XRT data not available. See Cadolle Bel *et al.* (2011) for more details.

was extremely bright in Swift/XRT ($>$ 400 cts s^{-1}).The JEM-X fluxes were around 370 mCrab and 240 mCrab in, respectively, the 3–10 and 10–20 keV energy bands, while the ISGRI fluxes were varying around 190 mCrab and 130 mCrab in the 20–40 keV and 40–80 keV energy bands. The X-ray source was softening. We fitted the closest XRT, PCA and IBIS/ISGRI spectra simultaneously with `XSPEC v12.6.0` (Arnaud 1996). The data were in general well-fitted using absorbed power-law (or cut-off power-law and Comptonisation) with reflection combined with a multicolour black-body, and a Gaussian Fe line at $\sim$ 6.5 keV. An example of the fitted spectra obtained during our *INTEGRAL* observations is shown in Fig. 2 (left). Table 1 summarizes the main spectral parameters for all observations. GX 339−4 reached the brightest magnitudes recorded on 2010 April 1, MJD 55287, just before the start of the transition from the LHS to softer states. During this LHS rise, the source brightened at a mean rate of $\sim$ 0.01 mag d^{-1} between MJD 55237–55287. Between MJD 55294–55297, the optical flux faded rapidly by $\sim$ 1 mag in 3.0 days (Russell *et al.* 2010) and a change in the SED to a bluer colour was observed. Months later, the optical and NIR brightnesses in all filters decreased. ATCA observations conducted on MJD 55283 showed flux densities $\sim$ 20 mJy with an inverted radio spectrum (spectral index spanning

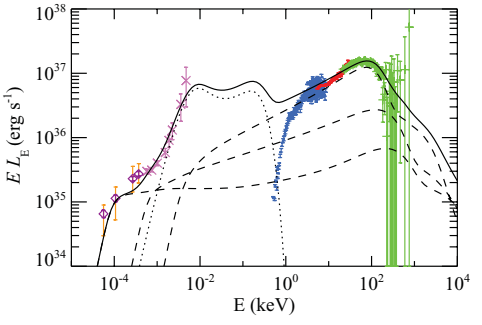

Figure 3. SED with the same data than in Figure 2 (right) fitted with the model of Veledina *et al.* (2012). Work in progress.

https://doi.org/10.1017/S1743921312019114 Published online by Cambridge University Press

+0.1 to +0.2, typical of powerful self-absorbed compact jets observed in LHS). On MJD 55372, no radio emission was detected at the location of GX 339−4: this was consistent with the source being in a soft state (Corbel *et al.* 2010). We refer to Cadolle Bel *et al.* (2011) for more details on the fitting and spectral parameter evolutions.

4. Discussion

Spectral analysis showed that the source transited from an initial LHS, with a spectrum dominated by Comptonisation in the beginning of the outburst (MJD $\sim$ 55217– 55281), to softer states where the power-law cut-off was not needed anymore and the photon index of the power-law was very soft ($\sim$ 2.3). In X-ray binaries, a cut-off power-law spectrum is usually interpreted as the signature of inverse Comptonisation of soft-seed photons by a thermalised population of electrons. In the LHS, we detected the compact core jet also in the optical/IR. We added radio flux data to the SED in Fig. 2 (right): it is remarkably similar to the Fig. 2 of Corbel & Fender (2002). One can interpret the results with a very rough approach: a simple power-law extrapolation of the radio data up to the NIR/optical clearly does not fit the data since an excess emission is seen. Similarly, several power-law components with distinct slopes are needed to fit later SEDs: after the LHS, the radio spectral index became typical of optically thin synchrotron radiation, probably as a result of freely expanding plasma blobs previously ejected (see, e.g., Fender *et al.* 2004); multiple ejection events took place during the outburst and then interacted with the interstellar medium (Corbel *et al.* 2010). Besides, we applied a hot flow model (Fig. 3) to describe the broadband spectra around MJD 55260. Finally, we clearly detected the jet evolution and its dramatic quenching at all wavelengths (for more details: Cadolle Bel *et al.* 2011, 2012).

References

Arnaud, K. A. 1996, ASP Conferences, 101, 17
Cadolle Bel, M., Kuulkers, E., Ibarra, A., *et al.* 2010, The Astronomer's Telegram, 2573, 1
Cadolle Bel, M., Prat, L., Rodriguez, J., *et al.* 2009, *A&A*, 501, 1
Cadolle Bel, M., Rodriguez, J., D'Avanzo, P., *et al.* 2011, *A&A*, 534, A119
Cadolle Bel, M., Rodriguez, J., D'Avanzo, P., *et al.* 2012, *A&A*, 544, C2
Chincarini, G., Zerbi, F., Antonelli, A., *et al.* 2003, The Messenger, 113, 40
Corbel, S., Broderick, J., Calvelo, D., *et al.* 2010, The Astronomer's Telegram, 2745, 1
Corbel, S. & Fender, R. P. 2002, *ApJ*, 573, L35
Coriat, M., Corbel, S., Buxton, M. M., *et al.* 2009, *MNRAS*, 400, 123
Covino, S., Stefanon, M., Sciuto, G., *et al.* 2004, in Presented at the Society of Photo-Optical Instrumentation Engineers (SPIE) Conference, Vol. 5492, Society of Photo-Optical Instrumentation Engineers (SPIE) Conference Series, ed. A. F. M. Moorwood & M. Iye, 1613–1622
Fender, R. P., Belloni, T. M., & Gallo, E. 2004, *MNRAS*, 355, 1105
Homan, J. & Belloni, T. 2005, Astrophysics and Space Science, 300, 107
Homan, J., Buxton, M., Markoff, S., *et al.* 2005, *ApJ*, 624, 295
McClintock, J. E. & Remillard, R. A. 2006, Black hole binaries, Compact stellar X-ray sources. Edited by Walter Lewin & Michiel van der Klis: Cambridge University Press, 157
Prat, L., Cadolle Bel, M., Terrier, R., *et al.* 2010, The Astronomer's Telegram, 2455, 1
Rodriguez, J., Shaw, S. E., Hannikainen, D. C., *et al.* 2008, *ApJ*, 675, 1449
Russell, D. M., Buxton, M., Lewis, F., & Altamirano, D. 2010, The Astronomer's Telegram, 2547, 1
Tanaka, Y. & Shibazaki, N. 1996, *ARAA*, 34, 607
Tomsick, J. A. 2010, The Astronomer's Telegram, 2384, 1
Veledina, A., Poutanen, J., & Vurm, I. 2012, ArXiv e-prints
Zerbi, F. M. & The Rem Team. 2001, in Astronomische Gesellschaft Meeting Abstracts, Vol. 18, Astronomische Gesellschaft Meeting Abstracts, ed. E. R. Schielicke, J101+

https://doi.org/10.1017/S1743921312019114 Published online by Cambridge University Press